Received: 27 February 2023 | Revised: 30 May 2023 | Accepted: 31 May 2023

DOI: 10.1002/pip.3724

RESEARCH ARTICLE

PROGRESS IN PHOTOVOLTAICS WILEY

Susceptibility to polarization type potential induced degradation in commercial bifacial p-PERC PV modules

Farrukh ibne Mahmood[1] | Fang Li[1] | Peter Hacke[2] | Cécile Molto[3] | Dylan Colvin[3] | Hubert Seigneur[3] | Govindasamy TamizhMani[1]

[1]Photovoltaic Reliability Laboratory, Arizona State University (ASU-PRL), Mesa, AZ, USA

[2]Reliability and System Performance, National Renewable Energy Laboratory (NREL), Golden, CO, USA

[3]Florida Solar Energy Center, University of Central Florida (UCF-FSEC), Cocoa, FL, USA

Correspondence
Farrukh ibne Mahmood, Photovoltaic Reliability Laboratory, Arizona State University (ASU-PRL), Mesa, AZ, USA.
Email: fmahmoo4@asu.edu

Funding information
U.S. Department of Energy (Office of Science, Office of Basic Energy Sciences and Energy Efficiency and Renewable Energy, Solar Energy Technology Program); Department of Energy, Office of Energy Efficiency and Renewable Energy, Grant/Award Number: DE-EE-0009345

Abstract

Potential induced degradation (PID) is a reliability issue affecting photovoltaic (PV) modules, mainly when PV strings operate under high voltages in hot/humid conditions. Polarization-type PID (PID-p) has been known to decrease module performance quickly. PID-p can be reduced or recovered under the light in some cases, but this effect, as expected, would be less pronounced on the rear side of bifacial PV modules receiving lower irradiance. As bifacial PV modules are projected to dominate the PV market within the next 10 years, it is crucial to understand the PID-p issue in bifacial modules better. In this study, we performed indoor PID testing to induce PID-p on 14 commercial bifacial p-PERC modules with three different module constructions from three manufacturers. Four rounds (+ve and −ve polarities for front and rear sides) of PID testing are done at 25°C, 54% relative humidity (RH) for 168 h using the aluminum foil method. Each module side (front cell side and back cell side) is tested individually under both negative and positive voltage bias. The results show that the highest degradation of 32% in maximum power (Pmax) at standard test conditions (1000 W/m^2) and 51% at low irradiance (200 W/m^2) has been observed in some cases. Recovery under sunlight is also done, and outcomes show a near-complete recovery in Pmax. This study presents an extensive experimental methodology and a detailed analysis to systematically and simultaneously/sequentially evaluate multiple construction types of bifacial modules to the PID-p susceptibility and recovery.

KEYWORDS
bifacial modules, indoor testing crystalline silicon, light recovery, photovoltaic reliability, PID, polarization, potential induced degradation, p-PERC

1 | INTRODUCTION

Increasing global energy demand, depletion of fossil fuels, and problems such as climate change have led to the growth of renewable energy technologies.[1–3] Solar energy is currently among the leading renewable energy technologies worldwide, and photovoltaics (PVs) is the most dominant technology within solar energy.[4] Traditionally, PV modules were constructed as such (glass–encapsulant–monofacial cell–encapsulant–backsheet) so that energy production was limited to the front side of a PV module.[5] Newer bifacial technologies (glass–encapsulant–bifacial cell–encapsulant–transparent backsheet or glass) allow power production from both the front and rear of a PV module.[6,7] Although additional power from the rear side increases the total module output, it presents new reliability challenges and issues.[8] Bifacial PV modules are projected to become the dominant PV technology in the coming years,[9–11] and the high reliability of these

modules is vital to ensure the long life of these types of modules and lower the LCOE.[12]

In the field, several reliability issues can damage the module, leading to lower power output or complete failure.[13–15] Potential induced degradation (PID) is a reliability issue reported in 2005 by Swanson et al.[16] that can develop when PV strings operate at high absolute voltages (1000–1500 V) under high temperature and humidity conditions.[17,18] The PID mechanisms can reduce module output by as high as 30%.[19,20]

Primarily, three types of PID mechanisms have been identified: PID-shunting (PID-s), PID-polarization (PID-p), and PID-corrosion (PID-c).[21,22] PID-s is caused by sodium (Na^+) ions drifting from the glass to the cell, leading to junction shunting. This results in a decrease in the shunt resistance (R_{SH}) and Fill Factor (FF).[23] PID-p can happen due to positive/negative charge accumulation in the dielectric/passivation layers leading to higher surface recombination and is characterized by a reduction in short circuit current (I_{SC}) and open circuit voltage (V_{OC}).[24] Moreover, PID-p has been reported as the fastest degradation mechanism among the different PID processes.[24] PID-c in bifacial p-PERC modules is linked to the corrosive effect caused by the oxygen in aluminum oxide (Al_xO_y), leading to the impairment of the Al_xO_y and silicon nitride (Si_xN_y) layers.[25] PID-c is non-recoverable, whereas PID-s is partially recoverable, and PID-p can be recovered completely.[26,27] For passivated emitter and rear contact (PERC) cells under a negative bias, the front side can experience PID-s,[28,29] and the rear can undergo PID-p[29,30] and PID-c.[25,29] When the cells are positively biased, the front side can suffer from PID-p[29,31]; for the rear side, there are few studies, and some report no PID mechanisms[29,32]; however, Sulas-Kern et al.[27] do report some degradation under positive bias at the rear of bifacial modules, and the modules were stressed for longer periods (1000 h) as compared to 168 h as done in this study. Since limited studies are available, it is imperative to understand the PID mechanisms on the rear and front of emerging bifacial PV technologies under negative and positive bias.

This study uses 3 types of commercial bifacial p-PERC PV modules, that, Glass–Glass Framed (GG-F), Glass-Transparent-Backsheet Framed (G-TBS-F), and Glass–Glass Non-Framed (GG-NF) from various manufacturers (total of 14 modules). The testing rounds are designed to focus on PID-p; however, other PID processes are also observed and examined. Four rounds of PID testing are done using the Al-foil method[33] to impact the modules' rear or front side with a positive or negative voltage bias. Flash IV (at high and low irradiances) and electroluminescence (EL) imaging are done pre and post-stress for each round on both module sides. Light recovery is carried out for those modules that experienced higher degradation to further understand the mechanism involved. Leakage current (LC) is also monitored through all rounds of PID stress testing.

So far, few papers have been published on the PID-p reliability issue of bifacial modules because the PID-p issue is a relatively new degradation mechanism in relatively new construction technology of bifacial modules. This study presents an extensive experimental methodology and a detailed analysis to systematically and simultaneously/sequentially evaluate multiple construction types of bifacial modules to the PID-p susceptibility and recovery.

It should be noted that this study's results only apply to modules tested in this investigation. The readers are cautioned that the findings reported in this study may not be generalized for all bifacial PERC modules currently available in the market. This study does not aim to compare different bifacial technologies but focuses on understanding PID-p susceptibility of bifacial modules with PERC cells on both rear and front sides individually under both positive and negative polarities.

2 | METHODOLOGY

The modules used in the study were purchased from an open market based on local availability; all samples are new. Fourteen commercial bifacial p-PERC modules were used, including three bifacial module constructions from three manufacturers. Details are given in Table 1. The modules were stressed for PID using the Al foil method (shown in Figure 1) at ±1500 V, 25°C, and 54% relative humidity (RH) (to simulate Arizona weather conditions) for 168 h in an indoor environmental chamber as per International Electrotechnical Commission (IEC) standard 62804-1. Four rounds of PID stress were conducted, each targeting a specific side of the module under a different polarity. The unstressed side of the module was kept at the same potential as the cell. This method was used so monofacial PID stress could be applied on the stressed side of the module and avoid stress on the non-stressed side.[32,34] For example, if the rear side is stressed at a negative voltage bias, the cells are at a negative bias, and the rear Al foil (stressed side) is grounded. In contrast, the front Al foil (unstressed side) is kept at the same potential as the cell, that is, negative bias. Due to module unavailability, M-B was reused in Rounds-3 and 4 after recovery (if applicable).

TABLE 1 Construction details of modules used in this study (GG = Glass-Glass; NF = Non Framed; F = Framed; TBS = Transparent Backsheet).

Manufacturer	Module name	Number of modules	Module construction	Cell type; dimensions	Encapsulant
A	MA	4	GG-NF (2 * 3.2-mm glass)	PERC-72-Full-cell; 156 × 156 mm	EVA
B	MB	2	GG-F (2 * 2.0-mm glass)	PERC-144- Half-cut cell; 78 × 156 mm	EVA
C	MC	4	G-TBS-F (3.2-mm glass)	PERC-144-Half-cut cell; 78 × 156 mm	EVA
A	MD	4	G-TBS-F (3.2-mm glass)	PERC-144-Half-cut cell; 78 × 156 mm	EVA

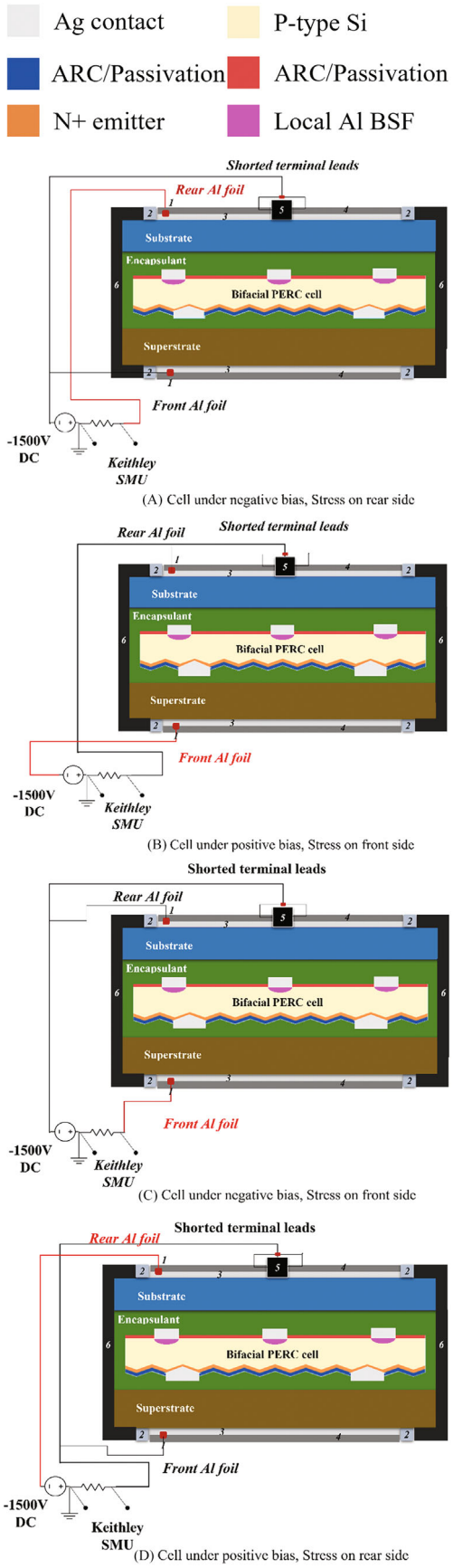

FIGURE 1 Experimental setup for (a) Round-1, (b) Round-2, (c) Round-3, and (d) Round-4; (#1) refers to Al tape connected between Al foil and the electrodes of the power supply, (#2) refers to insulation tape applied to the frame to prevent electrical connection between the rear substrate and the front superstrate, (#3) refers to Al foil that covers the front superstrate layer and rear substrate layer while keeping 1-cm distance toward the frame, (#4) refers to insulation mat for enabling a uniform surface contact of superstrate/substrate to the Al foil, (#5) refers to the junction box with shorted leads, and (#6) refers to the module frame. SMU refers to the source meter unit.

Table 2 shows the details of the PID testing. The module edges were covered with Kapton tape to avoid contact between the foil and the module frame (this was not an issue for frameless modules). Al sheets in small rectangular sizes (to ensure Al foil was in proper contact with the module surface) were placed on the front and rear of the modules (the front and rear Al sheets were not in contact), and 3M Al tape was used to ensure electrical connectivity between the small sheets. A thick and heavy insulating roofing membrane (thermoplastic polyolefin rubber membrane) was also attached to the front and rear of the modules on top of the Al foil to ensure firm and uniform contact between the Al foil and the module surfaces (front and rear sides). The modules were mounted horizontally on an electrically insulated stainless steel rack (inside a walk-in environmental chamber), as shown in Figure 2. Figure 1 shows the module testing configuration for each round of testing.

All modules employed in the experiment, including frameless modules, were prepared in a consistent manner, as detailed above. Although frameless modules may experience PID in the field significantly less due to the absence of a frame, the objective of this study was to explore the susceptibility of the cell type in the module laminate. By incorporating these module types, we ensured a comprehensive evaluation of various bifacial technologies currently available in the market, thus providing valuable insights into their performance and resilience under adverse conditions.

As mentioned, Rounds-1 to 4 were set up based on the review of PERC cell's susceptibility to PID-p (other PID mechanisms are also considered, but the focus is on PID-p). The first two rounds were designed to induce PID-p. The main focus is on these rounds, but round-3 was also performed to determine the contribution of PID-s under a negative bias on the front of the bifacial PERC module (application of stress to induce PID-p can simultaneously impact that). The fourth round was performed to see the impact of positive bias at the rear of the bifacial module. Table 2 summarizes these findings.

Before and after each round (or recovery), pre and post-characterization tests, including Flash IV and EL, were done to analyze the change in performance parameters. Flash IV was done using a Spire 5600 Single Long Pulse (SLP) solar simulator. The IV was carried out for both sides of each module at STC (1000 W/m^2) and low irradiance (200 W/m^2). Control modules were used to ensure the same

TABLE 2 PID testing polarity configuration and anticipated PID mechanisms according to the literature.[29]

Round	Cells polarity	Stressed side	Modules tested	Anticipated PID mechanisms in p-PERC cells according to literature
1	Negative (−ve)	Rear	MA-1, MB-1, MC-1, MD-1	PID-p,[27,28,31] PID-c[25,35,36]
2	Positive (+ve)	Front	MA-2, MB-2, MC-2, MD-2	PID-p[31]
3	Negative (−ve)	Front	MA-3, MB-1, MC-3, MD-3	PID-s[28,37,38]
4	Positive (+ve)	Rear	MA-4, MB-2, MC-4, MD-4	Reports some form of degradation but not fully understood[27] Few papers currently address this, and more work is needed[32]

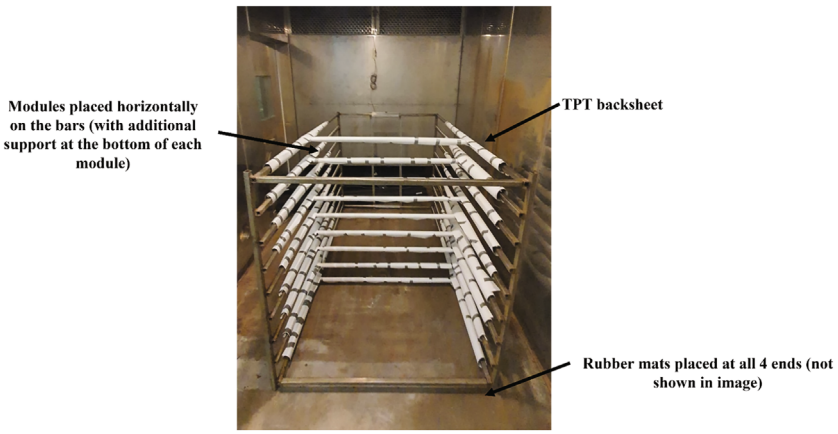

FIGURE 2 Rack for placing modules inside a walk-in environmental chamber, insulating backsheet material (white material) to the sides to prevent module's direct contact with the metallic rack, and rubber mats placed underneath the rack (not shown in the image) to avoid contact between the rack with the chamber.

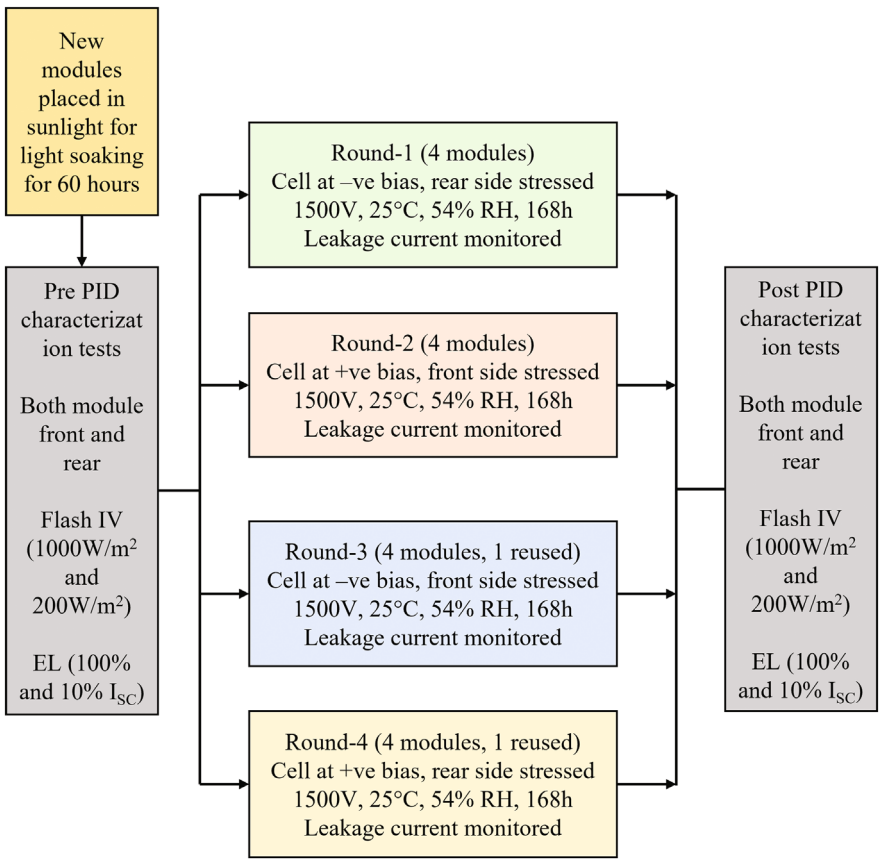

FIGURE 3 PID testing methodology used in this study.

settings throughout the study. IV parameters such as Pmax, FF, I_{SC}, V_{OC}, R_{SH}, and series resistance (R_S) were obtained through the Flash test. EL was carried out using a charge-coupled device (CCD) camera. The camera model used was Sensovation HR-830. EL for both module sides was done at 100% I_{SC} and 10% I_{SC} (for simplicity, only 100% I_{SC} results are presented), and the gray value using image analysis was also calculated.

A series of EL images were performed for the two heavily degraded modules (MA-1 and MB-1) at bias levels of 0.4A, 0.55A, 10%, 40%, 70%, and 100% of I_{SC}. These images were analyzed using the EL sweep method described in Colvin et al.[39] to extract the cell-level dark IV curves. These curves were subsequently analyzed using the model in Suckow et al.[40] for extracting R_S and the first diode recombination saturation current density (J_{01}). The LC for each round of PID stress was also recorded using a Keithley source meter (SMU).

The modules with the maximum degradation were also recovered under sunlight at open circuit conditions with an average dosage of 19.4 kWh/m^2 for the module front and 18.4 kWh/m^2 for the rear. Figure 3 summarizes the testing methodology for the study, and Figure 4 shows the recovery methodology. The color coding for Rounds-1 to 4 in Figure 3 corresponds with the PID mechanisms (as proposed in the literature) in Table 2.

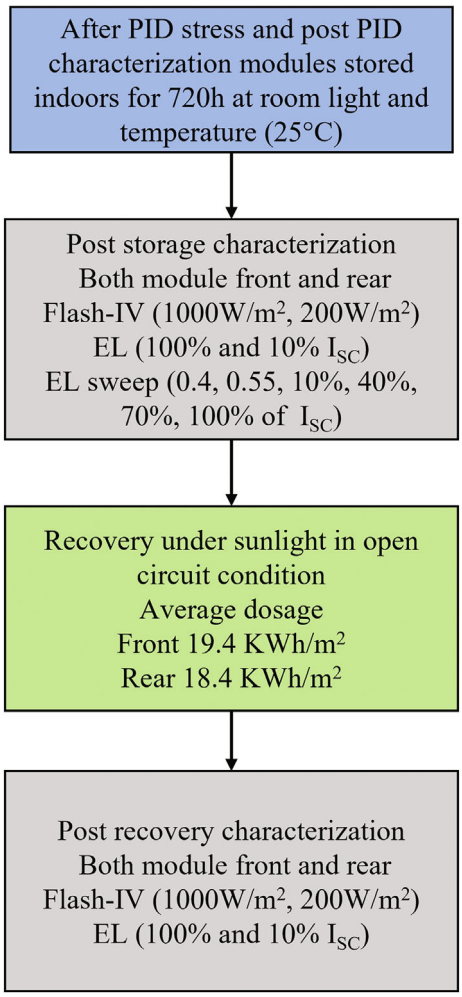

FIGURE 4 Recovery methodology for heavily degraded modules.

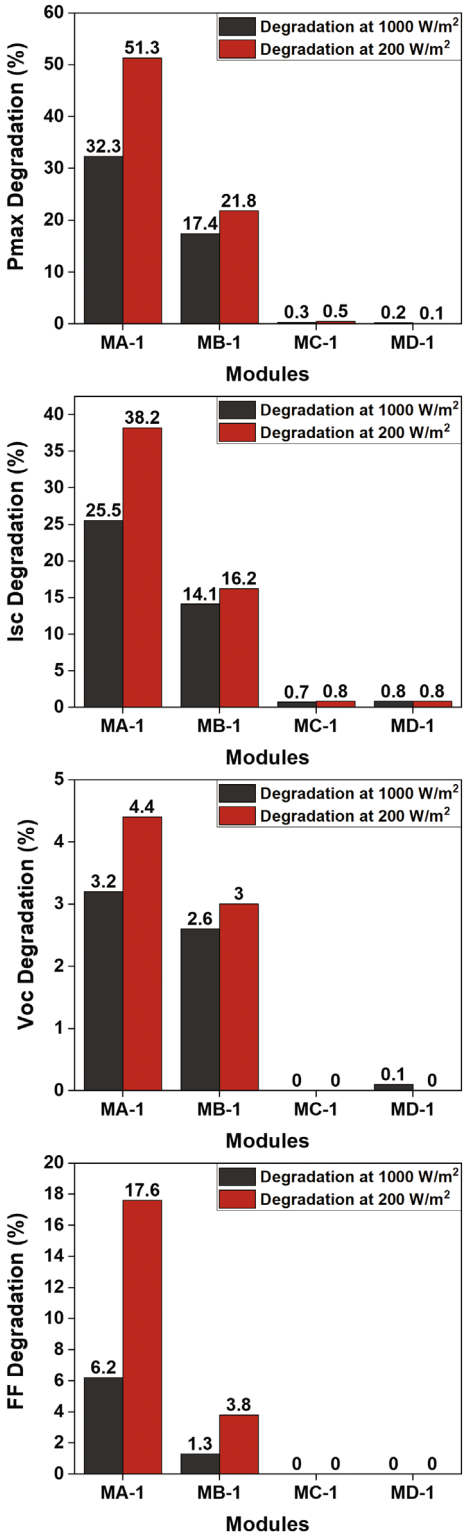

FIGURE 5 % degradation of IV parameters (rear stressed side) at STC and low irradiance (1000 and 200 W/m^2) after PID stress under a negative voltage bias on the rear side.

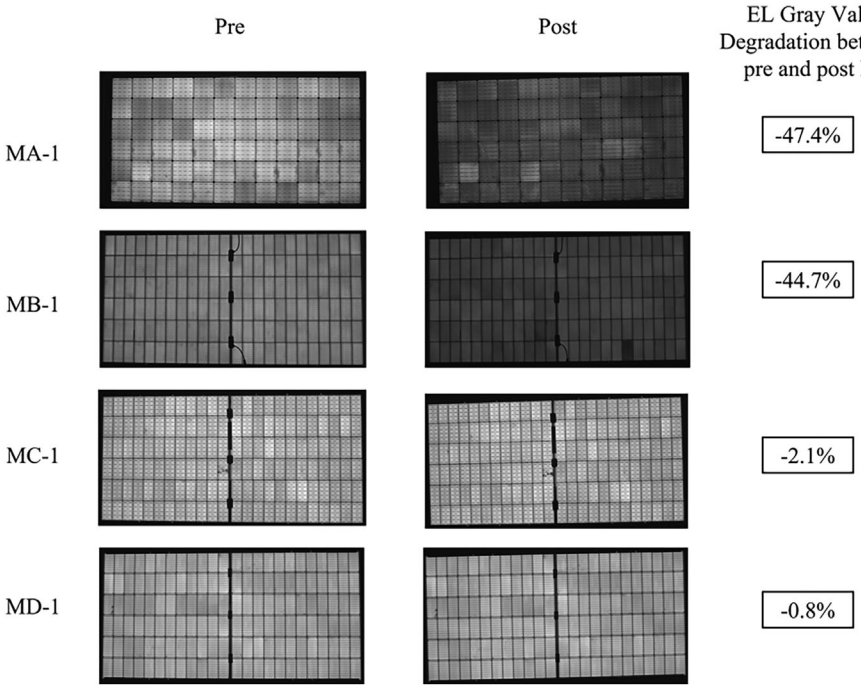

FIGURE 6 EL images at 100% I_{SC} and 30-s exposure before and after PID stress under a negative voltage bias on the rear side. The gray value change is given on the right side of the image.

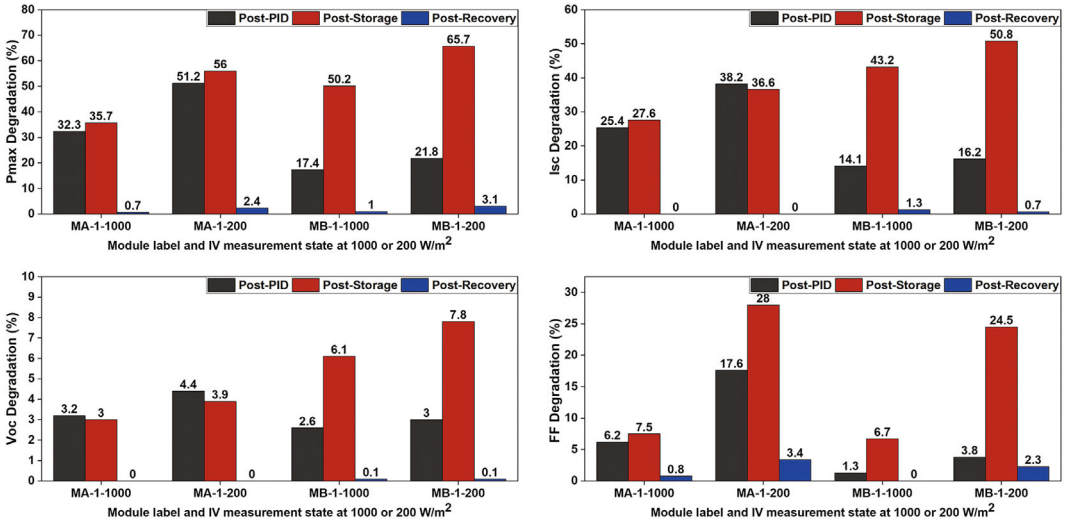

FIGURE 7 % degradation of IV parameters (rear stressed side) for MA-1 and MB-1 at STC and low irradiance (1000 and 200 W/m^2) after PID stress under a negative voltage bias on the rear side, after storage, and after light recovery.

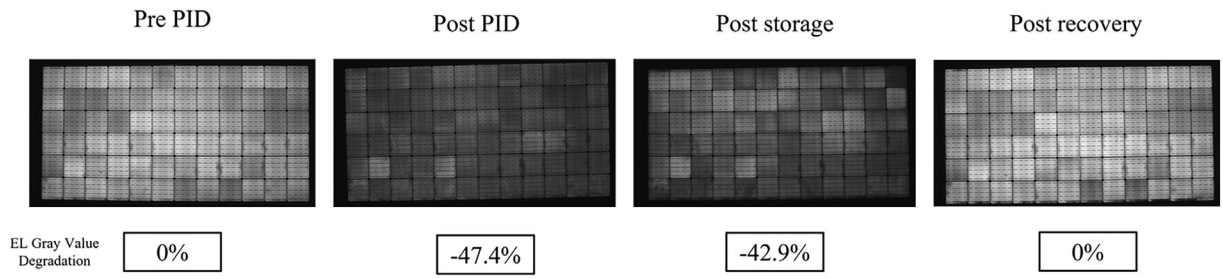

FIGURE 8 EL for MA-1 at different states for the rear side at 100% I_{SC} and 30s exposure with gray value change.

3 | RESULTS AND DISCUSSION

The percentage degradation between pre and post-characterization tests was calculated using the standard % change formula.

3.1 | Round-1 (cell at −ve bias and stress at rear side)

MA-1 and MB-1 were stored at room temperature and room light conditions for 720 h and then recovered under sunlight.

Results for Round-1, including IV and EL, suggest that under a negative bias with the stress at the rear side, a maximum degradation in Pmax of 32.3% and 17.4% for MA-1 and MB-1, respectively, be observed at STC. MA-1 and MB-1 are more susceptible to PID, and MC-1 and MD-1 degrade less than 1% in Pmax.

In Round-1, MC-1 and MD-1 might not be degrading because of the insulating properties of the backsheet. We observe that G-TBS modules (applicable to only the modules used in this study) are initially more resistant to PID on their rear side. This does not mean that these modules will be PID-resistant during field operation. The backsheet may be speculated to degrade over time, impacting the resistivity and increasing the module's sensitivity to PID. This will be the subject for future studies: inducing PID on the rear side of G-TBS modules after a prior degradation of the backsheet (damp heat, for instance).

The degradation in MA-1 and MB-1 can be attributed to PID-p since a significant drop is observed in I_{sc} (25.5% for MA-1 and 14.1% for MB-1 at STC), characteristic of PID-p. EL also confirms these findings as each cell's intensity decreases homogeneously. Also, an increase in R_s of 50.9% for MA-1 and 11.7% for MB-1 measured at low irradiance IV is observed. The average LC for MA-1 and MB-1 is also high, that is, 1.06×10^{-1} uA for MA-1 and 1.48×10^{-1} uA for MB-1 compared to 8.79×10^{-3} uA for MC-1 and 1.83×10^{-2} uA for MD-1. The IV data (post-PID) and EL images for MA-1 and MB-1 (pre and post-PID) are the same in Figures 5 and 6 and in Figures 7–9. This is done to compare post-storage and post-recovery data for MA-1 and MB-1.

Moreover, near-complete Pmax recovery for MA-1 and MB-1 further supports a PID-p mechanism. A possible mechanism is suggested in Luo et al.[32] When the cells are negatively biased, an electric field is created and oriented toward the cells. Consequently, positive charges are accumulated in the dielectric layers, which reduces the field-effect passivation on the rear p^+ side of p-PERC modules. This results in increased surface recombination velocity as attested by the Pmax degradation mainly due to I_{SC} decrease. It has been suggested that a polarization mechanism can involve the change of charge state of the K center in the SiN_x layer.[32,41] A K center is created via a Si dangling connection connected to three N atoms. K centers (K^0, K^-, or K^+) can be electrically neutral, negatively, or positively charged. The K^+/K^0 can absorb electrons, or the K^-/K^0 can release electrons under a voltage bias. Pre-PID, the K-center charge states in SiN_y are randomly distributed, and the passivation layer has a negative charge. K^-/K^0 releases electrons under the PID stress, which causes the K-center charge states in SiNy to change from negative to positive.[41,42] This increases the surface recombination velocity, causing a reduction in the module's power output, as described above.

The degradations are more severe when IV parameters are obtained at lower irradiance (200 W/m^2). This is linked to the change in the surface charge density of dielectric layers due to PID-p progression that leads to a shift in the rear surface recombination injection-level dependence.[32] Furthermore, for sufficiently doped p-type silicon,[43] the surface recombination velocity declines with rising carrier concentration. The quantity of fixed charge in the passivation layer further complicates the injection-level dependent recombination behavior. The effective surface recombination velocity increases then decreases again because of inversion as the positive charge density in the rear dielectric rises.[43]

Since degradation is more pronounced at low irradiance, the rear side of bifacial p-PERC modules is at a higher risk of PID-p, as they receive less light. This effect varies depending on the albedo on the rear surface where the modules are installed. Hence as less light reaches the rear side, the light recovery effect is also diminished, increasing the rear side's susceptibility to exhibiting PID-p. Another interesting result observed is further degradation in IV parameters in MB-1 during storage time before recovery. The EL sweep (performed after storage) results for the rear and front sides of MA-1 and MB-1 are shown in the Supporting Information in section A. A greater J_{01} for MA-1 in specific cells indicates max degradation, but a lower J_{01} is displayed in other cells, suggesting partial recovery. With EL sweep images for MB-1, the same outcome is revealed. Although Flash IV and EL data post-storage for MA-1 indicate that there was less Pmax loss compared to MB-1. The detailed effect of change in J_{01} and R_S

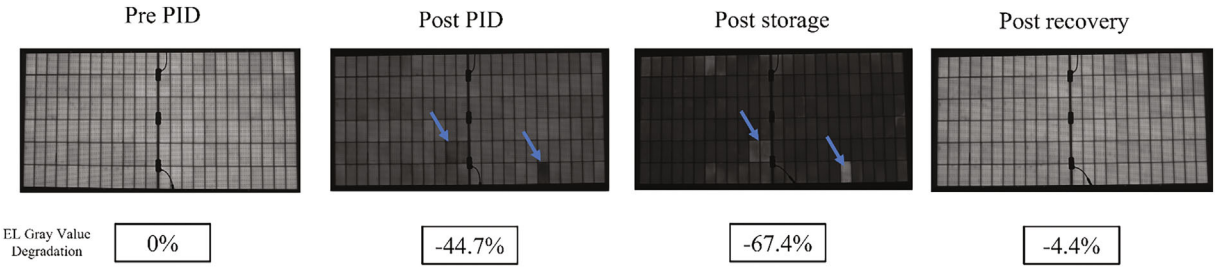

FIGURE 9 EL for MB-1 at different states for the rear side at 100% I_{SC} and 30s exposure with gray value change.

due to PID-p reflected in EL sweeps will be explored in detail in future studies.

Moreover, EL in Figure 9 shows partial recovery in some cells (blue arrows). MA-1, on the other hand, shows almost the same degradation levels post-storage as observed post-PID in the EL. This process can be explained by the studies done in Luo et al. and Sporleder et al.[32,42] They suggest three PID stages in progression. The initial stage is (A). The point of lowest Isc is referred to as the degraded state (or B), and the state of improved Isc after further voltage stress is referred to as the regenerated state (or C). The regenerated state C corresponds to an inversion layer on the cell's rear. For MA-1, the module has reached near complete degradation after PID and is near B. After storage, the state is between A and B because we can see the EL recover slightly, indicating light recovery. For MB-1 post PID, the module state is toward C, regeneration, and after storage, most cells reach B (complete degradation, darker EL images show degradation).

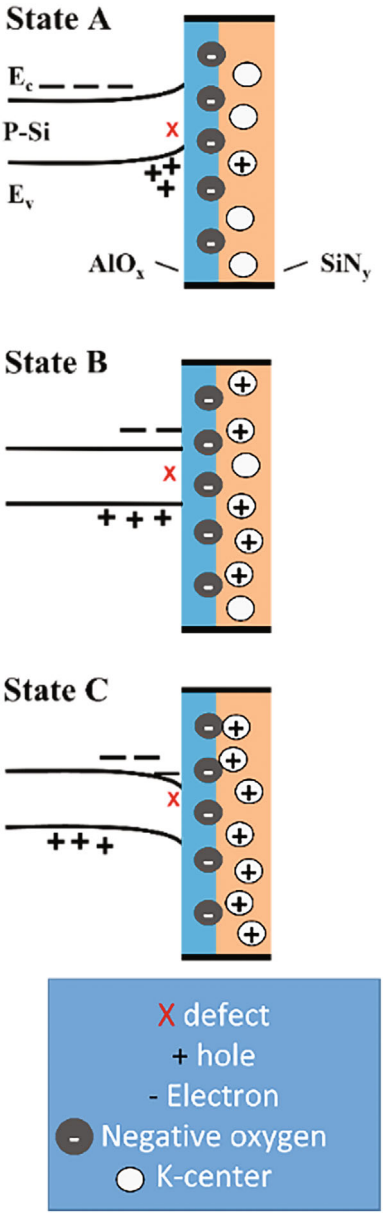

FIGURE 10 Representation of impact of charge distributions at presumed states A, B, and C on energy band bending (reconstructed from Sporleder et al.[42]).

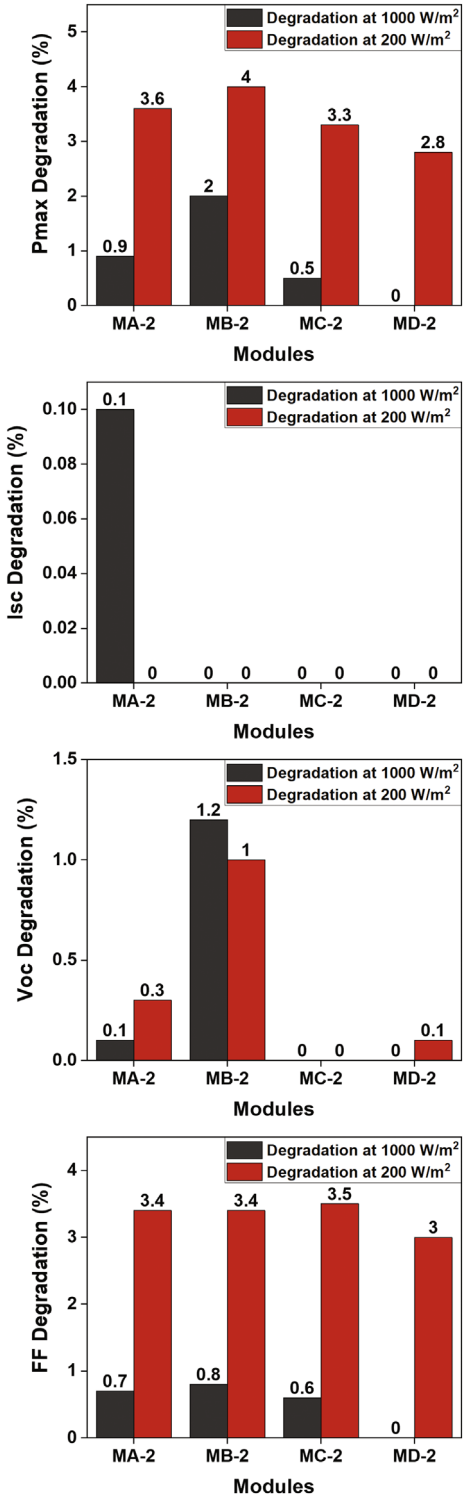

FIGURE 11 % degradation of IV parameters (front stressed side) at STC and low irradiance (1000 and 200 W/m^2) after PID stress under a positive voltage bias applied to the cells.

However, some cells move closer to state B after PID stress and recover toward A during storage, as shown by blue arrows in Figure 9. After sunlight recovery, both modules reach state A.[42] A reason for not observing the inversion stage in MA-1 can be a difference in the passivation of both modules. Figure 10 demonstrates the energy band bending for the 3 states reconstructed from Sporleder et al.[42]

3.2 | Round-2 (cell at +ve bias and stress at the front side)

In round-2, degradation in Pmax in all modules is less than 5%, as shown in Figure 11. EL also supports these results, as shown in Figure 12. R_S and R_{SH} measured using low irradiance IV show a 0.8% increase in R_S and a 15.5% decrease in R_{SH} for MA-2. MB-2 shows no change in R_S and a 14% reduction in R_{SH}. For MC-2, R_S increases by 9.2%, and R_{SH} decreases by 20.9. MD-2 has no change in R_S and a 20.6% decline in R_{SH}. Average LC for MA-2, MB-2, MC-2, and MD-2 are 4.77×10^{-2}, 1.37×10^{-1}, 6.75×10^{-3}, and 7.60×10^{-2} uA, respectively.

We attribute the degradation in Round-2 to PID-p as well. Although significant degradation in I_{SC} is not observed but using data presented in Figures 13 and 14 for the traditional glass white backsheet (G-WBS) module (with bifacial PERC cells), we can argue that the mechanism responsible for degradation when the cell is at a positive bias with respect to the front side is PID-p. ME-1 is a glass-backsheet (monofacial) module from manufacturer D employing bifacial p-PERC cells (144-half-cut cells 78 × 156 mm).

The results for ME-1 are included separately to maintain consistency of module type as all are bifacial modules, but the results are included here individually to explain the PID mechanism for round-2. ME-1 was subjected to the same PID conditions as the other 4 modules in Round-2. Since degradation was too low for the other 4 modules, recovery was not done for them. Therefore, results for ME-1, which included an additional recovery step, were necessary to understand the recovery process and the PID mechanism involved in Round-2.

ME-1 almost completely recovers under sunlight. Since the stress is under a positive bias, the mechanism cannot be PID-s as the Na^+ ion is involved, which cannot be driven into the junction at a positive bias. PID-c, on the other hand, is an irreversible process. Therefore, complete recovery coupled with positive bias stress suggests a PID-p mechanism for Round-2. Furthermore, the front side of p-PERC under positive bias is rarely studied in the literature. Theoretically, due to a positive bias at the front of p-PERC, PID-p can occur due to the drift of negative charges toward the cell. Also, light recovery results further consolidate the observation that the mechanism responsible is PID-p. Furthermore, PID-p mechanisms on the front and rear can also differ due to differences in the charges involved in the process and doping, as the rear side is less doped than the front emitter. This could explain why the significant loss in power is coming from FF rather than I_{SC}, as is usually seen in PID-p on the rear.

3.3 | Round-3 (cell at −ve bias and stress at the front side)

MB-1 was reused in Round-3 after light recovery. All other modules (MA-3, MC-3, MD-3) showed less than a 1% decline in Pmax for both

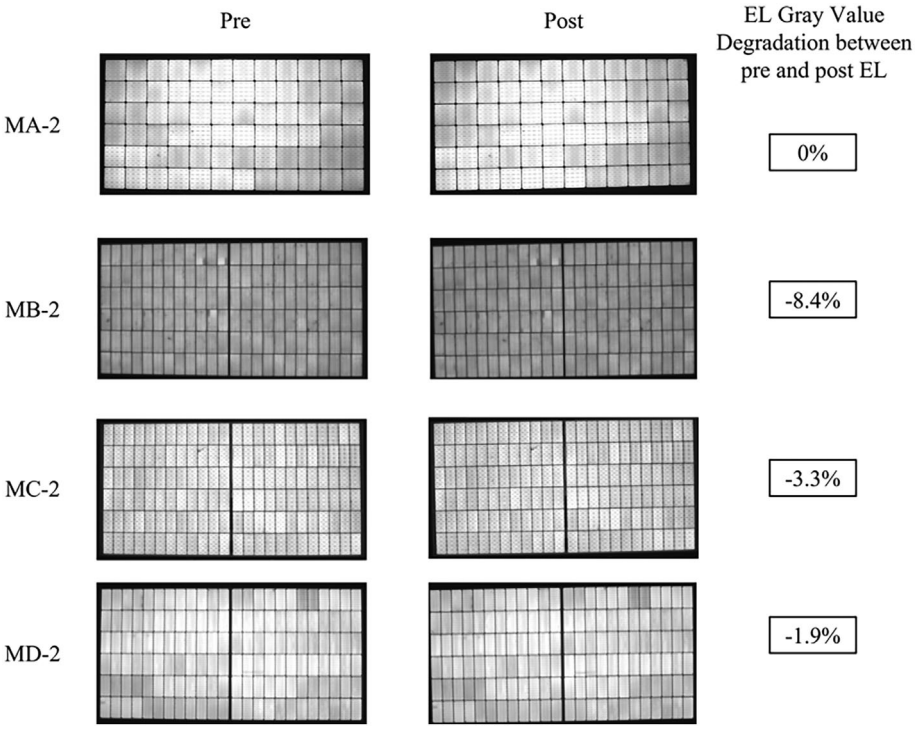

FIGURE 12 EL images at 100% I_{SC} and 30s exposure before and after PID stress under a positive voltage bias on the front side. The gray value change is given on the right.

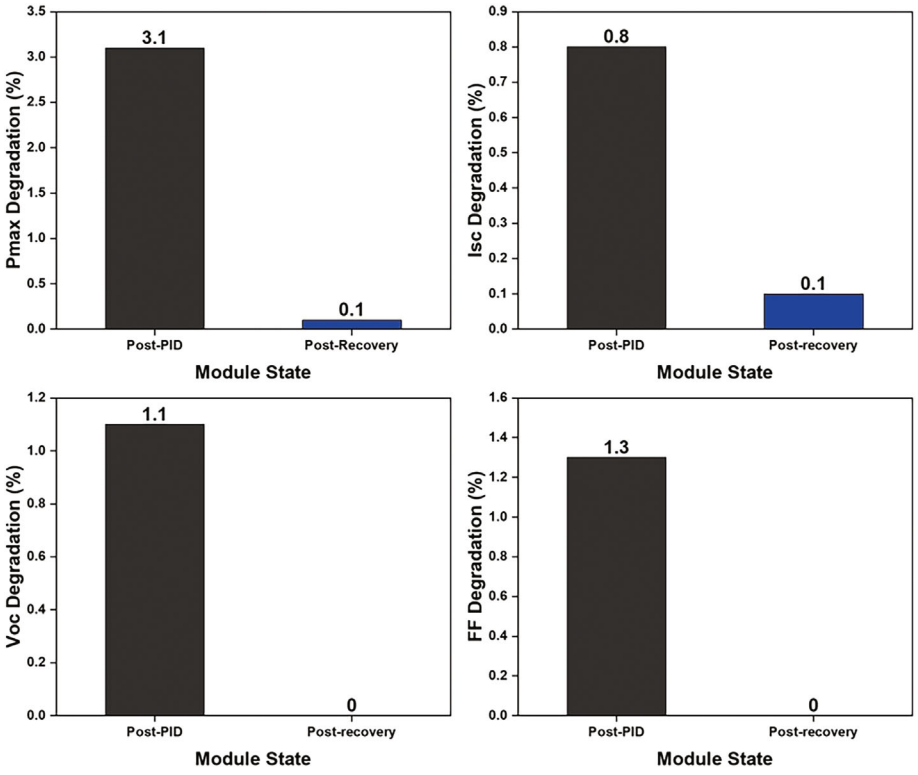

FIGURE 13 Degradation and recovery in IV parameters due to PID for ME-1 at 1000 W/m^2.

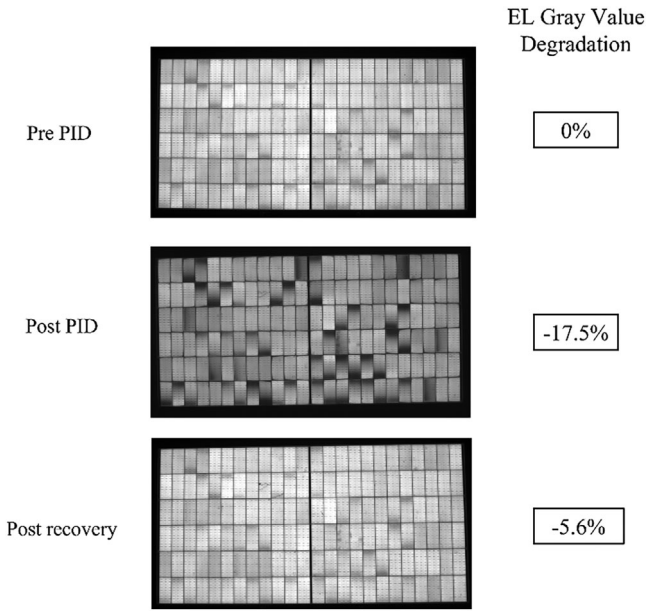

FIGURE 14 EL for ME-1 at different states at 100% I_{SC} and 30-s exposure with gray value change in Round-2 testing.

stressed and unstressed sides (at 1000 and 200 W/m^2), indicating no degradation.

Results for MB-1 are shown in Table 3. Interestingly, the degradation is mainly observed on the unstressed side. A slight reduction of the EL intensity is observed, as reported in Figure 15.

The % change in R_S and R_{SH} at the stressed side at 200 W/m^2 is +12.1% and −14.0%, respectively. The average LC for 168 h of test duration was 1.65×10^{-1} uA.

In Round-3, degradation is only observed in MB-1, and other modules degrade less than 1% in Pmax. Under a negative bias at the front of the PERC cell, the degradation can be due to PID-s. The reductions in FF and R_{SH} also support this hypothesis that PID-s might occur on the front side, even though the impact is not very pronounced. However, more degradation is observed at the module rear (unstressed side) than at the front side. We attribute this to two reasons. One reason can be the reuse of MB-1 in Round-3. However, the module was used after recovery. Still, stress for 168 + 168 h in both rounds can lead to moisture ingress in the module, as suggested by EL, indicating more cell darkening at the module edges. Hence, moisture penetration can also lead to stress on the unstressed rear side.

Also, moisture ingress can occur in the edge sealant leading to an additional path for the LC to the module's rear side. This leads to another hypothesis that some LC may reach the rear side on the edges of the module (even though the front side is tested). In that case, we could have some PID-p on edge responsible for the edge darkening in EL images. Hence, unintentionally PID-p could be occurring at the module rear, and we could see the effects of that on the front side. This could explain more degradation on the rear unstressed side compared to the front stressed side. Both these hypotheses will be explored in more detail in future studies to understand the mechanisms (either PID-s or PID-p) leading to the degradation of the unstressed side of the modules in this round.

Flash test side	% Pmax change	% I_{sc} change	% V_{oc} change	% FF change
Front-1000 W/m^2	−0.2	−0.1	−0.1	−0.1
Front-200 W/m^2	−0.8	−0.2	−0.1	−0.5
Rear-1000 W/m^2	−6.4	−0.2	−0.2	−5.9
Rear-200 W/m^2	−8.0	−0.9	−0.2	−7.0

TABLE 3 % change in IV parameters for stressed (front) and unstressed (rear) side at 1000 and 200 W/m^2 for MB-1 (reused after recovery) in Round-3 testing.

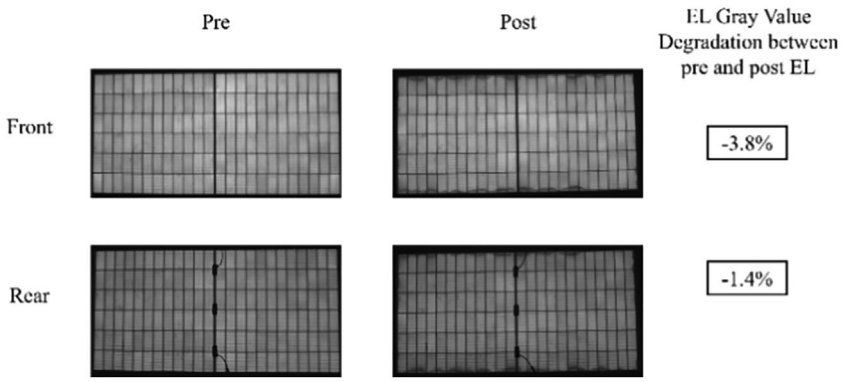

FIGURE 15 EL images and % gray value degradation for stressed (front) and unstressed (rear) side for MB-1 (reused after recovery in Round-1) at 100% I_{SC} and 30-s exposure.

Moreover, the monofacial PID stress method for bifacial modules using the Al foil is still under testing, and these results indicate some limitations of this method.

3.4 | Round-4 (cell at +ve bias and stress at rear side)

All modules showed less than a 1% decline in Pmax for both stressed and unstressed sides (at 1000 and 200 W/m^2), indicating no degradation. No significant difference in EL intensity is reported.

The case of the p-PERC module stressed under a positive bias at the rear side is barely studied in the literature. This study confirms that PID is unlikely to occur. Based on theoretical analysis, PID processes related to Na^+ ions (PID-s and PID-c due to SiO_x formation at the Si/AlO_x interface) cannot occur at a positive bias where Na^+ ions are drifted away from the cells. PID-p can also be excluded as the accumulation of negative charges at the rear p^+ side will enhance the passivation properties rather than degrade them. It is worth mentioning that PID-c due to metallic contact corrosion could eventually happen under a positive bias but for longer stress durations and in damp heat conditions (1000 to 2000 h under damp heat).[44,45]

This round of study also suggests that the GG modules are more prone to PID on their rear side than G-TBS modules. This is also reported in other studies.[5,28] The main reason is the insulating property of the transparent backsheet, preventing LC and, therefore, PID impacts. However, these results may not be generalized for all GG and G-TBS modules available in the market. Moreover, this study does not aim to compare GG and G-TBS modules since modules are from different manufacturers and have different bills of materials. We studied a limited number of modules, and the results only apply to these tested modules.

4 | CONCLUSIONS

An extensive experimental methodology and a thorough analysis of PID susceptibility in commercial PERC c-Si bifacial modules are presented in this study. We observed that the maximum degradation in bifacial modules in Pmax due to PID-p was seen when the cell is at a negative bias with respect to the rear side (32% at 1000 W/m^2). This degradation was more severe at lower irradiances (51% at 200 W/m^2), which is critical to understanding bifacial modules' effectiveness as the rear sides are exposed only to lower irradiances. Degradation was also observed in one of the modules after storage before recovery under natural sunlight. Under sunlight (about 18 kWh/m^2), near-complete recovery was observed in all modules. When the cell was under a positive bias with respect to the module front, the degradation was less than 5%, and we attribute this loss to the PID-p process. When the cell is under a negative bias with respect to the front, we believe a PID-s mechanism could be responsible for Pmax degradation in the module. However, more degradation on the unstressed side also suggests that it could be an unintentional PID-p process at the rear leading to a leaching effect at the front side. Future studies will be aimed at confirming the mechanism under these circumstances. When the cell is at the positive bias with respect to the module rear, degradation in all modules in Pmax is less than 1%, practically indicating the absence of any PID process. Some supporting results are included in the Supporting Information to keep the paper concise. The presented results suggest that PID-p may be observed in bifacial PERC module technologies currently available in the market.

The readers are cautioned that the findings reported in this study have some limitations, such as a statistically small sample size that may not fully represent the entire bifacial market. The modules used were purchased from a few select manufacturers based on local availability, and the findings should not be generalized for all bifacial PERC

modules currently available in the market since distinct manufacturers can have modules with different bills of materials. The study utilized controlled laboratory conditions to simulate PID stress, which may not perfectly replicate real-world conditions where environmental factors and temperature fluctuations can influence PID susceptibility.

AUTHOR CONTRIBUTIONS

Farrukh ibne Mahmood, the corresponding author, played a major role in the design of the experiment, conducted the main experimental work, and performed the analysis of results. He was also primarily responsible for writing the manuscript and overseeing any necessary revisions. Fang Li contributed to the methodology and experimental work and also participated in revising the manuscript. Peter Hacke, alongside Hubert Seigneur and GovindaSamy TamizhMani, was involved in the conceptualization of the project, procuring the necessary funding, design of experiment, and manuscript revisions. Cecile Molto contributed to the experimental methodology and provided necessary revisions to the manuscript. Dylan Colvin was primarily involved in conducting EL sweep experiments and formulating the associated methodology. All authors have read and approved the final version of the manuscript.

ACKNOWLEDGEMENTS

This material is based upon work supported by the Department of Energy, Office of Energy Efficiency and Renewable Energy (EERE), under Award Number DE-EE-0009345. We would like to thank SolarPTL, LLC, for allowing us to perform the flash I-V tests reported in this paper.

DATA AVAILABILITY STATEMENT

The data that support the findings of this study are available on request from the corresponding author. The data are not publicly available due to privacy or ethical restrictions.

ORCID

Farrukh ibne Mahmood https://orcid.org/0000-0001-8540-9144
Fang Li https://orcid.org/0000-0003-1556-4215
Peter Hacke https://orcid.org/0000-0003-4850-0947
Hubert Seigneur https://orcid.org/0000-0002-5047-4541

REFERENCES

1. Dincer I. Renewable energy and sustainable development: a crucial review. *Renew Sustain Energy Rev*. 2000;4(2):157-175. doi:10.1016/S1364-0321(99)00011-8
2. Ali S, Ali A, Saher S, Agha HS, bin Abdul Majeed H, Mahmood FI, TamizhMani G. A Comprehensive Study of 18–19 years field Aged modules for Degradation Rate Determination along with defect Detection and Analysis Using IR, EL, UV. In 2018 15th International Bhurban Conference on Applied Sciences and Technology (IBCAST); 2018:28-35.
3. Asad M, Mahmood FI, Baffo I, Mauro A, Petrillo A. The cost benefit analysis of commercial 100 MW solar PV: the plant Quaid-e-Azam Solar Power Pvt Ltd. *Sustain*. 2022;14(5):1-13, 2895. doi:10.3390/su14052895
4. Bojek P. IEA Solar PV. 2022.
5. Sinha A, Sulas-Kern DB, Owen-Bellini M, et al. Glass/glass photovoltaic module reliability and degradation: a review. *J Phys D Appl Phys*. 2021;54(41):413002. doi:10.1088/1361-6463/ac1462
6. Saw MH, Khoo YS, Singh JP, Wang Y. Enhancing optical performance of bifacial PV modules. *Energy Procedia*. 2017;124:484-494. doi:10.1016/j.egypro.2017.09.285
7. ibne Mahmood F, Kumar A, Afridi M, Tamizhmani G. Potential induced degradation in c-Si glass-glass modules after extended damp heat stress. *Sol Energy*. 2023;254:102-111. doi:10.1016/j.solener.2023.03.013
8. Zhang Y, Yu Y, Meng F, Liu Z. Experimental investigation of the shading and mismatch effects on the performance of bifacial photovoltaic modules. *IEEE J Photovoltaics*. 2019;10(1):296-305. doi:10.1109/JPHOTOV.2019.2949766
9. Kopecek R, Libal J. Bifacial photovoltaics 2021: status, opportunities and challenges. *Energies*. 2021;14(8):2076. doi:10.3390/en14082076
10. International Technology Roadmap for Photovoltaic (ITRPV) 2020 Results; 2020.
11. Afridi M, Kumar A, ibne Mahmood F, Tamizhmani G. Hotspot testing of glass/backsheet and glass/glass PV modules pre-stressed in extended thermal cycling. *Sol Energy*. 2023;249:467-475. doi:10.1016/j.solener.2022.12.006
12. Gu W, Ma T, Ahmed S, Zhang Y, Peng J. A comprehensive review and outlook of bifacial photovoltaic (bPV) technology. *Energ Conver Manage*. 2020;223:113283. doi:10.1016/j.enconman.2020.113283
13. Sharma V, Chandel S. Performance and degradation analysis for long term reliability of solar photovoltaic systems: a review. *Renew Sustain Energy Rev*. 2013;27:753-767. doi:10.1016/j.rser.2013.07.046
14. Raza HA, Mahmood FI, TamizhMani G. Use of non-contact voltmeter to quantify potential induced degradation in CdTe modules. *Sol Energy*. 2023;252:284-290. doi:10.1016/j.solener.2023.02.002
15. Mahmood F, Majeed H, Agha H, et al. Temperature coefficient of power (Pmax) of field aged PV modules: impact on performance ratio and degradation rate determinations. In Reliability of Photovoltaic Cells, Modules, Components, and Systems X, 2017, pp. 52–58.
16. Swanson R, Cudzinovic, M, DeCeuster D, et al. The surface polarization effect in high-efficiency silicon solar cells. In 15th PVSEC; 2005.
17. Pingel S, Frank O, Winkler M, et al. Potential induced degradation of solar cells and panels. In 2010 35th IEEE Photovoltaic Specialists Conference, 2010:002817-002822.
18. Bouaichi A, Merrouni AA, el Amrani A, et al. Long-term experiment on p-type crystalline PV module with potential induced degradation: impact on power performance and evaluation of recovery mode. *Renew Energy*. 2022;183:472-479. doi:10.1016/j.renene.2021.11.031
19. Dhimish M, Badran G. Recovery of photovoltaic potential-induced degradation utilizing automatic indirect voltage source. *IEEE Trans Instrum Meas*. 2021;71:1-9. doi:10.1109/TIM.2021.3134328
20. ibne Mahmood F, Tamizhmani G. Impact of different backsheets and encapsulant types on potential induced degradation (PID) of silicon PV modules. *Sol Energy*. 2023;252:20-28. doi:10.1016/j.solener.2023.01.047
21. Luo W, Khoo YS, Hacke P, et al. Potential-induced degradation in photovoltaic modules: a critical review. *Energ Environ Sci*. 2017;10(1):43-68. doi:10.1039/C6EE02271E
22. Mahmood FI, TamizhMani G. Impact of anti-soiling coating on potential induced degradation of silicon PV modules. In 2022 IEEE 49th Photovoltaics Specialists Conference (PVSC); 2022:1198-1200.
23. Naumann V, Lausch D, Hähnel A, et al. Explanation of potential-induced degradation of the shunting type by Na decoration of stacking faults in Si solar cells. *Sol. Energy Mater. Sol. Cells*. 2014;120:383-389. doi:10.1016/j.solmat.2013.06.015
24. Yamaguchi S, Van Aken BB, Stodolny MK, Löffler J, Masuda A, Ohdaira K. Effects of passivation configuration and emitter surface

doping concentration on polarization-type potential-induced degradation in n-type crystalline-silicon photovoltaic modules. *Sol Energy Mater sol Cells*. 2021;226(February):111074.
25. Sporleder K, Bauer J, Groser S, et al. Potential-induced degradation of bifacial PERC solar cells under illumination. *IEEE J. Photovoltaics*. 2019;9(6):1522-1525. doi:10.1109/JPHOTOV.2019.2937231
26. Koch S, Nieschalk D, Berghold J, Wendlandt S, Krauter S, Grunow P. Potential induced degradation effects on crystalline silicon cells with various antireflective coatings. In Proceedings of the 27th European Photovoltaic Solar Energy Conference and Exhibition, Frankfurt; 2012:24-28.
27. Sulas-Kern DB, Owen-Bellini M, Ndione P, et al. Electrochemical degradation modes in bifacial silicon photovoltaic modules. *Prog Photovolt Res Appl*. 2022;30(8):948-958. doi:10.1002/pip.3530
28. Carolus J, Tsanakas JA, van der Heide A, Voroshazi E, De Ceuninck W, Daenen M. Physics of potential-induced degradation in bifacial p-PERC solar cells. *Sol Energy Mater sol Cells*. 2019;200:109950. doi:10.1016/j.solmat.2019.109950
29. Molto C, Oh J, Mahmood FI, et al. Review of potential-induced degradation in bifacial PV modules. *Energ Technol*. 2023;11(4):2200943. doi:10.1002/ente.202200943
30. Sporleder K, Turek M, Schüler N, Naumann V, Hevisov D, Hagendorf C. Quick test for reversible and irreversible PID of bifacial PERC solar cells. *Sol Energy Mater sol Cells*. 2021;219(September 2020):110755.
31. Jonai S, Nakamura K, Masuda A. Universal explanation for degradation by charge accumulation in crystalline Si photovoltaic modules with application of high voltage. *Appl Phys Express*. 2019;12(10):101003. doi:10.7567/1882-0786/ab3cf7
32. Luo W, Hacke P, Terwilliger K, et al. Elucidating potential-induced degradation in bifacial PERC silicon photovoltaic modules. *Prog Photovoltaics Res Appl*. 2018;26(10):859-867. doi:10.1002/pip.3028
33. IEC TS 62804–1: 2015 Photovoltaic (PV) modules-Test methods for the detection of potential-induced degradation-Part 1: Crystalline silicon. IEC--International Electrotech. Comm Ed, vol. 1, 2015.
34. Carolus J, Breugelmans R, Tsanakas JA, et al. Why and how to adapt PID testing for bifacial PV modules? *Prog Photovolt Res Appl*. 2020;28(10):1045-1053. doi:10.1002/pip.3311
35. Sporleder K, Naumann V, Bauer J, et al. Local corrosion of silicon as root cause for potential-induced degradation at the rear side of bifacial PERC solar cells. *Phys Status Solidi Rapid Res Lett*. 2019;13(9):1900163. doi:10.1002/pssr.201900163
36. Sporleder K, Naumann V, Bauer J, et al. Microstructural analysis of local silicon corrosion of bifacial solar cells as root cause of potential-induced degradation at the rear side. *Phys Status Solidi*. 2019;216(17):1900334. doi:10.1002/pssa.201900334
37. Naumann V, Hagendorf C, Grosser S, Werner M, Bagdahn J. Micro structural root cause analysis of potential induced degradation in c-Si solar cells. *Energy Procedia*. 2012;27:1-6. doi:10.1016/j.egypro.2012.07.020
38. Hacke P, Smith R, Terwilliger K, Perrin G, Sekulic B, Kurtz S. Development of an IEC test for crystalline silicon modules to qualify their resistance to system voltage stress. *Prog Photovoltaics Res Appl*. 2014;22(7):775-783. doi:10.1002/pip.2434
39. Colvin DJ, Schneller EJ, Davis KO. Cell dark current–voltage from non-calibrated module electroluminescence image analysis. *Sol. Energy*. 2022;244:448-456. doi:10.1016/j.solener.2022.08.043
40. Suckow S, Pletzer TM, Kurz H. Fast and reliable calculation of the two-diode model without simplifications. *Prog Photovolt Res Appl*. 2014;22(4):494-501. doi:10.1002/pip.2301
41. Yamaguchi S, Nakamura K, Masuda A, Ohdaira K. Rapid progression and subsequent saturation of polarization-type potential-induced degradation of n-type front-emitter crystalline-silicon photovoltaic modules. *Jpn J Appl Phys*. 2018;57(12):122301. doi:10.7567/JJAP.57.122301
42. Sporleder K, Naumann V, Bauer J, Turek M, Hagendorf C. Potential induced degradation studies with high temporal resolution reveal changes of field effect passivation states at the rear side of bifacial silicon solar cells. In 2021 IEEE 48th Photovoltaic Specialists Conference (PVSC); 2021:935-938.
43. Aberle AG, Glunz S, Warta W. Impact of illumination level and oxide parameters on Shockley–Read–Hall recombination at the Si-SiO2 interface. *J Appl Phys*. 1992;71(9):4422-4431. doi:10.1063/1.350782
44. Hacke P, Kempe M, Terwilliger K, et al. Characterization of multicrystalline silicon modules with system bias voltage applied in damp heat. In Proc. 25th European Photovoltaic Solar Energy Conference and Exhibition/5th World Conf. Photovoltaic Energy Conversion; 2010:3760.
45. Brecl K, Bokalic M, Topic M. Examination of photovoltaic silicon module degradation under high-voltage bias and damp heat by electroluminescence. *J Sol. Energy Eng Trans ASME*. 2017;139(3):1-6. doi:10.1115/1.4036056

SUPPORTING INFORMATION

Additional supporting information can be found online in the Supporting Information section at the end of this article.

How to cite this article: Mahmood Fi, Li F, Hacke P, et al. Susceptibility to polarization type potential induced degradation in commercial bifacial p-PERC PV modules. *Prog Photovolt Res Appl*. 2023;31(11):1078-1090. doi:10.1002/pip.3724